Conformational Dynamics of Loop 262−274 in G- and F-actin†

Alexander Shvetsov,‡ John D. Stamm,§,|| Martin Phillips,‡ Dora Warshaviak,‡ Christian Altenbach,§ Peter A. Rubenstein,⊥ Kálmán Hideg,# Wayne L. Hubbell,§ and Emil Reisler*,‡

Department of Chemistry and Biochemistry and Molecular Biology Institute, University of California, Los Angeles, Los Angeles, California 90095, Department of Biochemistry, University of Iowa College of Medicine, Iowa City, Iowa 52242, Jules Stein Eye Institute and Department of Chemistry and Biochemistry, University of California, Los Angeles, Los Angeles, California 90095, and Institute of Organic and Medicinal Chemistry, University of Pécs, H-7602 Pécs, Hungary

Received December 15, 2005; Revised Manuscript Received February 16, 2006

ABSTRACT: According to the original Holmes model of F-actin structure, the hydrophobic loop 262−274 stabilizes the actin filament by inserting into a pocket formed at the interface between two protomers on the opposing strand. Using a yeast actin triple mutant, L180C/L269C/C374A [$(LC)_2CA$], we showed previously that locking the hydrophobic loop to the G-actin surface by a disulfide bridge prevents filament formation. We report here that the hydrophobic loop is mobile in F- as well as in G-actin, fluctuating between the extended and parked conformations. Copper-catalyzed, brief air oxidation of $(LC)_2CA$ F-actin on electron microscopy grids resulted in the severing of thin filaments and their conversion to amorphous aggregates. Disulfide, bis(methanethiosulfonate) (MTS), and dibromobimane (DBB) cross-linking reactions proceeded in solution at a faster rate with G- than with F-actin. Cross-linking of C180 to C269 by DBB (4.4 Å) in either G- or F-actin resulted in shorter and less stable filaments. The cross-linking with a longer MTS-6 reagent (9.6 Å) did not impair actin polymerization or filament structure. Myosin subfragment 1 (S1) and tropomyosin inhibited the disulfide cross-linking of phalloidin-stabilized F-actin. Electron paramagnetic resonance measurements with nitroxide spin-labeled actin revealed strong spin−spin coupling and a similar mean interspin distance (∼10 Å) in G- and in F-actin, with a broader distance distribution in G-actin. These results show loop 262−274 fluctuations in G- and F-actin and correlate loop dynamics with actin filament formation and stability.

The ability of actin monomers (G-actin)[1] to self-associate reversibly into double-stranded helical filaments (F-actin) and the dynamic modulation of this process are key elements of cellular life (*1*, *2*). Many factors and proteins accelerate or inhibit various steps in filament formation, branching, bundling, or severing (*3*, *4*). The detailed understanding of these processes requires the knowledge of atomic structures and dynamics of G- and F-actin. While the structure of G-actin is well established and has been solved by several groups, all considerations of F-actin structure depend on the original model of Holmes et al. (*5*) or its variants (*6*, *7*). In the structure of the actin monomer (G-actin), residues 262−274 form a hydrophobic loop located between subdomains 3 and 4 (*5*, *8*). In their original model of F-actin, Holmes et al. (*5*) hypothesized that during actin polymerization this loop moves away from the surface of the protein in a direction perpendicular to the filament axis. According to this model (*5*), the hydrophobic loop inserts into a pocket formed by the interface of two protomers on the opposing strand of the helix, thereby stabilizing the actin filament. The motion of the loop, or at least its detachment from the G-actin surface that is implicit in this model, was supported by normal mode analysis of the actin structure (*9*). Moreover, several studies with loop mutants of yeast actin highlighted both the role of this loop in actin polymerization (*10*−*12*) and its dynamic nature (*13*−*15*).

In a recent study Shvetsov et al. (*16*) devised a direct test of hydrophobic loop detachment from the G-actin surface during actin polymerization. These authors prepared a triple $(LC)_2CA$ yeast actin mutant which places two cysteine residues in positions enabling the locking of loop 262−274 to the monomer surface via a disulfide bond. According to the G-actin structure and the F-actin model (*5*, *8*) these cysteines (Cys-180 and Cys-269) are predicted to be separated by ∼10 Å in F-actin and ∼5.9 Å in G-actin. Disulfide cross-linking of C180 to C269 on G-actin blocked (reversibly) filament formation, resulting in its polymerization into amorphous aggregates and providing evidence for

† This work was supported by grants from the USPHS (AR 22031) and NSF (MCB 0316269) to E.R., the USPHS (GM 33689) to P.A.R., the USPHS (EY 05216) and the Jules Stein Professor Endowment to W.L.H., and the USPHS (Training Grant T32 EY07026) to J.D.S. and was also partially supported by a grant to K.H. from the Hungarian National Research Foundation (OTKA TO 48334).

* To whom correspondence should be addressed. Telephone: (310) 825-2668. Fax: (310) 206-7286. E-mail: reisler@mbi.ucla.edu.

‡ Department of Chemistry and Biochemistry and Molecular Biology Institute, UCLA.

§ Jules Stein Eye Institute and Department of Chemistry and Biochemistry, UCLA.

|| Present address: Department of Physics, University of Evansville, Evansville, IN 47722.

⊥ Department of Biochemistry, University of Iowa College of Medicine.

Institute of Organic and Medicinal Chemistry, University of Pécs.

[1] Abbreviations: $(LC)_2CA$, yeast actin mutant (L180C/L269C/C374A); MTS, bis(methanethiosulfonate); DBB, dibromobimane; DNase I, deoxyribonuclease I; F-actin, filamentous actin; G-actin, monomer actin; S1, myosin subfragment 1; Tm, tropomyosin; DTT, dithiothreitol.

10.1021/bi052558v CCC: $33.50
Published on Web 04/27/2006

Scheme 1

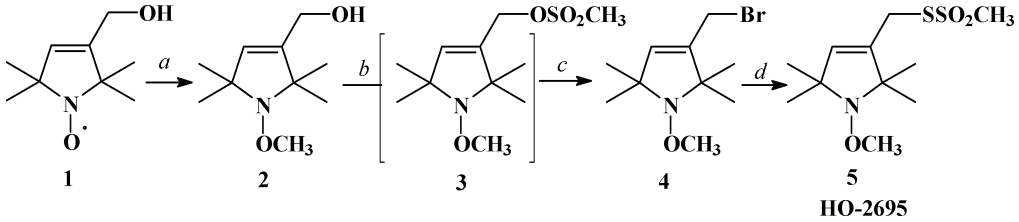

a mandatory displacement for the hydrophobic loop during the G- to F-actin transition. Disulfide cross-linking of C180 to C269 was observed also in F-actin, leading to filament destruction. However, it was not clear whether cysteine oxidation did not occur in the actin monomer pool, thereby driving F-actin depolymerization. In a more recent study we have provided electron microscopy evidence for C180−C269 disulfide formation in actin filaments and their severing under mild oxidative conditions (*17*). In this work, we have used the disulfide, dibromobimane (DBB), and bis(methanethiosulfonate) (MTS 1, 3, 4, 6, and 8) cross-linkers of increasing span (0−12 Å) as a ruler to assess the range of dynamic motions of loop 262−274 and to determine the distances between cysteines 180−269 which favor a stable filament structure. We show that while locking the hydrophobic loop in the parked, monomer-like conformation by a C180−C269 disulfide in F-actin destabilizes and disrupts the filaments, cross-linking these cysteines in G- and F-actin with reagents of increasing length causes progressively less filament impairment. The results of our cross-linking experiments and electron paramagnetic resonance (EPR) measurements with nitroxide spin-labeled $(LC)_2CA$ actin also show that the hydrophobic loop is mobile in F-actin, albeit less than in G-actin, fluctuating between the detached and parked conformations.

EXPERIMENTAL PROCEDURES

Materials and Reagents. Bis(methanethiosulfonate) (MTS) cross-linking reagents MTS-1 [1,1-methanediyl bis(methanethiosulfonate)], MTS-3 [1,3-propanediyl bis(methanethiosulfonate)], MTS-4 [1,4-butanediyl bis(methanethiosulfonate)], MTS-6 [1,6-hexanediyl bis(methanethiosulfonate)], and MTS-8 [3,6-dioxaoctane-1,8-diyl bis(methanethiosulfonate)] were purchased from Toronto Research Chemicals Inc. (North York, Ontario, Canada). Dibromobimane (DBB) was obtained from Calbiochem (a brand of EMD Biosciences, Inc., La Jolla, CA). Peptone, tryptone, and yeast extract were from Difco (Detroit, MI). DNase I grade D was purchased from Worthington Biochemical Corp. (Lakewood, NJ). Affi-gel-10 and Bio-Rad protein assay (Bradford assay) were obtained from Bio-Rad (Hercules, CA). Sephadex G-50, NEM, ATP, phalloidin, DTT, and PMSF were purchased from Sigma Chemical Co. (St. Louis, MO). Vivaspin 0.5 mL concentrators with 10000 MWCO PES membrane were obtained from Viva Science (Hannover, Germany). The methanethiosulfonate spin-labeling reagent [(1-oxy-2,2,5,5-tetramethylpyrrolinyl-3-methyl)methanethiosulfonate (MTSL)] was synthesized as previously described (*18*). A diamagnetic analogue [(1-methoxy-2,2,5,5-tetramethylpyrrolinyl-3-methyl)methanethiosulfonate] was prepared according to Scheme 1.

Compound **1** (*19*) was treated with methylmagnesium iodide (2.2 equiv) in diethyl ether at 0 °C, the reaction mixture warmed to room temperature, and after 1 h the resultant mixture was extracted with a saturated aqueous solution of NH_4Cl. The ether phase was dried (anhydrous $MgSO_4$), the solvent was evaporated, and compound **2** was obtained in 70% yield as a colorless solid. To a solution of **2** in CH_2Cl_2 at 0 °C were added triethylamine (2.2 equiv) and methanesulfonyl chloride (2.2 equiv). The solution was warmed to room temperature, and after 1 h LiBr (4.0 equiv) in acetone was added, and the mixture was warmed to 55 °C for 1 h to give **3** in 55% yield. To a solution of **3** in acetone/water was added $NaSSO_2CH_3$ (4.0 equiv), and the mixture was left to stand for 30 min at 55 °C to give **5** as white crystals in 75% yield (mp 51−52 °C).

Site-Directed Mutagenesis. The preparation of actin mutants L269C/C374A and L180C/L269C/C374A was described in previous publications (*15*, *16*). The creation of L180C/C374A mutant actin followed our established procedures, using the QuikChange site-directed mutagenesis kit (Stratagene, La Jolla, CA) and centromeric plasmid pRS314 (*20*) marked with the *TRP1* gene. The oligodeoxynucleotide used to generate the mutation L180C in L269C/C374A actin was 5′-GAGAATCGATTGTGCCGGTAGAG-3′ (the mutant codon is underlined). Yeast transformation with this plasmid was carried out as described before (*15*).

Proteins. Yeast actin was purified by affinity chromatography on a DNase I column as described before (*13*). Purified G-actin was stored in 10 mM Tris-HCl (pH 8.0), 0.2 mM $CaCl_2$, 0.2 mM ATP, and 1.0 mM DTT on ice and was used within 3 days from the completion of the preparation. F-actin was prepared by polymerizing G-actin with 3.0 mM $MgCl_2$ and an equimolar amount of phalloidin (*16*). The concentration of actin was measured by the Bradford protein assay using skeletal rabbit muscle actin as a standard.

Myosin subfragment 1 (S1) was prepared by chymotryptic digestion of myosin by the method of Weeds and Pope (*21*). Tropomyosin was purified as described by Smillie (*22*).

Cross-Linking of Actin and SDS−PAGE Analysis. We used bis(methanethiosulfonate) cross-linking reagents (MTS-1, -3, -4, -6, and -8) as a molecular ruler to assess the range of dynamic motions of loop 262−274 and to determine the distances between cysteines 180−269 that favor a stable filament structure. These reagents (MTS-1 through MTS-8) span a cross-linking distance range from 5.4 to 12.1 Å. Molecular dynamic simulations of the cross-linkers (DBB and MTS-1 through MTS-8) were performed using the CVFF force field as implemented in the Insight II (Accelrys, Inc.) program, at 298 K, for 2.5 ns with 1.5 fs time intervals. Every picosecond the cross-linking distance was measured. The average, median, and mode (most probable) distances were calculated for each cross-linker from the distances measured during the simulation.

Immediately prior to cross-linking reactions, DTT was removed from G-actin by passing the actin solution over Sephadex G-50 spin columns equilibrated with 10 mM MOPS buffer (pH 7.2), 0.2 mM $CaCl_2$, and 0.2 mM ATP. Cysteines 180 and 269 on G- and F-actin were cross-linked on ice or at room temperature for the indicated times (1−30 min), either via disulfide bond formation, using 5−20 μM $CuSO_4$ to catalyze air oxidation, or with 10−20 μM MTS reagents and 20 μM DBB (4.4 Å span). Aliquots of these reactions were withdrawn from the mixture at selected time points. Free cysteine residues were blocked in these aliquots with 2.0 mM NEM. Cross-linking of $(LC)_2$CA G- and F-actin resulted in its complete transformation into species with higher electrophoretic mobility on SDS−PAGE in the absence of mercaptoethanol. Actin samples were analyzed on 7.5% SDS−PAGE (*23*).

Actin Polymerization Assays. Actin polymerization was monitored via light scattering measurements in a SPEX Fluorolog fluorometer set at 325 nm for both excitation and emission wavelengths. The polymerization was induced by adding 3.0 mM $MgCl_2$ and equimolar amounts of phalloidin to G-actin.

Electron Microscopy. Samples of actin freshly polymerized with 3.0 mM $MgCl_2$ and equimolar amounts of phalloidin, either un-cross-linked (with 1.0 mM DTT) or cross-linked, were diluted with the polymerizing buffer to 2.5 μM immediately before being spread onto carbon-coated grids. The preparation of electron microscopy grids followed the previously reported procedure (*24*). Negatively stained actin samples were observed in a Hitachi H-7000 electron microscope. To assess the effect of C180−C269 disulfide cross-linking on filament structure, DTT-free $(LC)_2$CA actin filaments freshly adsorbed to the grid were exposed to a brief (up to 5 min), copper-catalyzed air oxidation. This involved placing a drop of actin polymerization buffer (free of DTT) containing 20 μM $CuSO_4$ on the grid for the selected times.

Spin-Labeling of Actin and EPR Spectroscopy. Prior to spin-labeling, DTT was removed from G-actin by passing it over Sephadex G-50 spin columns equilibrated with 10 mM MOPS buffer (pH 7.2), 0.2 mM $CaCl_2$, and 0.2 mM ATP. G-actin (20−25 μM) was incubated in the same buffer with a 3-fold molar excess of MTSL or a mixture of MTSL and the diamagnetic analogue (2:1 mole ratio) for 1 h on ice. Unreacted label was removed from the samples using the same Sephadex G-50 gel filtration columns, and if needed, the actin was concentrated using Vivaspin 0.5 mL concentrators (Viva Science, Hannover, Gemany) with a 10000 MWCO PES membrane. Samples of freshly spin-labeled G-actin were polymerized for 20 min at room temperature with 3.0 mM $MgCl_2$ and equimolar amounts of phalloidin. Labeling stoichiometry of these samples was checked by MALDI mass spectrometry. Compared with unlabeled actin, the labeled actin *m*/*z* values were shifted by 370 Da, revealing 2:1 mole ratio of the spin probe to actin. *m*/*z* values corresponding to partial (1:1) actin labeling were not detected in MALDI spectra. Spectra of G- and F-actin were recorded at X-band microwave frequencies using either a Bruker E580 spectrometer (Bruker Biospin, Billerica, MA) fitted with a 4119HS cavity or a Varian 109 spectrometer fitted with a two-loop one-gap resonator (LGR) (*25*). Samples were contained in a Suprasil flat cell (volume 40 μL; Wilmad, Buena, NJ) or a glass capillary (volume 5 μL; VitroCom, Inc., Mountain Lakes, NJ) for each spectrometer, respectively. Spectra were collected with a 160 G field scan, a modulation amplitude of 4 G at 100 kHz, and an incident microwave power of either 10 mW (4119HS) or 2 mW (LGR). The recorded data are averages of typically 20−60 30 s scans.

Measurement of Interspin Distance. Altenbach et al. (*26*) showed that distances between two spin-labels can be determined at room temperature using an application of rigid lattice theory in cases where the overall rotational correlation time of the protein, and thus the interspin vector, is slow (*26*). Briefly, the EPR spectrum of a molecule with an interacting pair of spin-labels is assumed to be a convolution of the spectrum with no spin−spin interactions with a broadening function that depends on the distance between the labels (*27*). This broadening function is fit to a weighted sum of Pake functions (*28*) and the distance distribution calculated from the known distance dependence of the Pake functions. Assuming that static dipolar interactions rather than relaxation effects due to loop motion dominate the spectral broadening in G-actin, the apparent interspin distance distribution can be obtained by the convolution methods previously described (*26*). The fitting and distance determination was facilitated by software written in LabVIEW (National Instruments, Austin, TX) by Christian Altenbach (*26*).

The MTSL reagent or a mixture containing a 2:1 molar ratio of the MTSL:diamagnetic analogue was used as described above to generate samples for the interacting and noninteracting spectra, respectively. Assuming equal reactivity and quantitative reaction, 8/9 of the actin molecules labeled with the mixture will have one or zero paramagnetic centers. Therefore, only 1/9 of the molecules will yield the interacting spectrum, and this component can be easily subtracted.

Molecular Dynamic Simulation Modeling of the Spin-Labeled G-actin. The crystal structure of *Saccaromyces cerevisiae* actin in complex with gelsolin segment-1 (PDB ID code 1YAG) was used as starting point for the model. Residues Leu-180 and Leu-269 were mutated to cysteines in silico, and MTSL probe molecules were attached to L180C and L269C through a disulfide bond. Energy minimizations and molecular dynamic simulations were performed in vacuo with the CVFF force field using the Discover module of Insight II software (Accelrys, Inc.) on a Silicon Graphics Octane workstation. Only the loop (262−274) backbone and side chains and the side chain of the residue 180 were allowed to move; the rest of the protein was fixed. The minimization procedure consisted of 300 steps of steepest descent followed by quasi-Newton−Raphson minimization until convergence. MD simulation was performed at 300 K for 10 ps with 1 fs time intervals after minimization. Every picosecond the distance between the nitrogen atoms of the MTSL reagents at positions 180 and 269 was measured.

Modeling of Disulfide, DBB, and MTS-6 Cross-Linked F-actin. The Holmes F-actin model showing three actin monomers (PDB code 3actin; *7*) was used as the starting model. Atoms within 30 Å radius around the 262−274 loop were used in the calculations. Residues Leu-180 and Leu-269 were mutated to cysteines in silico and cross-linked by a disulfide bridge or using DBB or MTS-6 cross-linkers. Energy minimizations were performed in vacuo with the

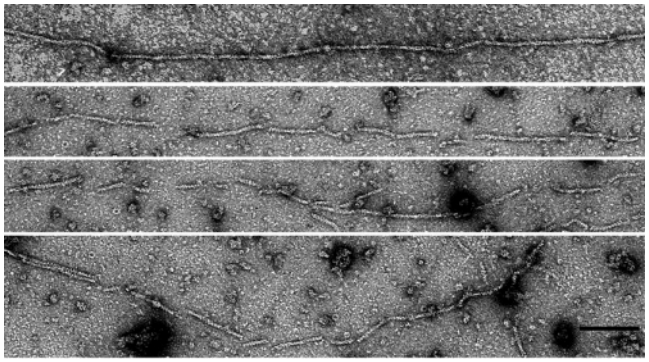

FIGURE 1: Representative images of oxidized actin filaments. After adsorption to EM grids the filaments were exposed to a brief (2.5 min) copper-catalyzed oxidation. The top lane shows the control, unoxidized filament; the lower three lanes represent oxidized actin. The oxidation resulted in destabilization and severing of filaments as well as the appearance of amorphous actin aggregates. The bar corresponds to 1000 Å.

CVFF force field using the Discover module of Insight II software (Accelrys, Inc.) on a Silicon Graphics Octane workstation. The cross-linked structures were minimized for 300 steps of steepest descent followed by quasi-Newton−Raphson minimization until convergence. During the minimization, only the loop (262−274) backbone and side chains and the side chain of the residue 180 were allowed to move, and the rest of the protein was kept fixed.

RESULTS

Locking of the Hydrophobic Loop in the Parked, Monomer-like State in F-actin Results in the Destabilization and Severing of Actin Filaments. According to the original Holmes model of F-actin structure (*5*), the hydrophobic loop 262−274 stabilizes the actin filament by inserting into a pocket formed at the interface between two protomers on the opposing strand. The connection between the two long-pitch F-actin strands might be a key for the control of F-actin stabilization. To study the proposed role and dynamics of the hydrophobic loop, we used $(LC)_2CA$, L269C/C374A, and L180C/C374A yeast actin mutants. This mutation places two cysteine residues in positions allowing the locking of loop 262−274 to the surface of the same monomer via a disulfide bond. In the previous study we found that Cys-180 and Cys-269 can form a disulfide bond in F-actin (*16*), in which, according to the original Holmes F-actin model (*5*), the distance between these cysteines should not favor such a reaction. EM revealed that such a disulfide cross-linking in F-actin in solution resulted in filament destruction and formation of amorphous aggregates. We hypothesized that the most probable mechanism is that of local dynamic instability within the filaments, with the hydrophobic loop fluctuating between the detached, and parked, monomer-like conformation. To examine this hypothesis in a greater detail in the current study, we used disulfide (zero span), DBB (4.4 Å), and increasing length MTS (5.4−12.1 Å) cross-linking to block or constrain the motion of the loop in F-actin. We used these cross-linkings as molecular rulers to assess the range of proposed dynamic motions of the loop and to study the effect of these cross-links on filament structure and stability.

Figure 1 shows results of disulfide cross-linking experiments and EM observations. The hydrophobic loop in the $(LC)_2CA$ actin filament was locked by disulfide cross-linking of C180−C269 into a conformation unfavorable for filament stability. This cross-linking reaction was carried out on EM grids as described in Experimental Procedures. Samples of $(LC)_2CA$ actin were freshly polymerized with 3.0 mM $MgCl_2$ and stabilized by equimolar amounts of phalloidin. The uncross-linked sample (Figure 1, top lane; under reducing conditions) was diluted with polymerizing buffer to 2.5 μM immediately before being spread onto carbon-coated grids and negatively stained with uranyl acetate. For cross-linking, a drop of actin polymerizing buffer (free of DTT) containing 20 μM $CuSO_4$ was placed over actin on the grid to catalyze air oxidation of these cysteines. Electron micrographs demonstrate that locking of the hydrophobic loop in the parked, monomer-like state in F-actin (by disulfide bridging) results in the destabilization and fragmentation of actin filaments. Figure 1 (bottom three lanes) shows that brief (2.5 min), copper-catalyzed, air oxidation of F-actin on the grids caused severing and fragmentation of the filaments. Grids with adsorbed F-actin floated on a buffer that did not contain $CuSO_4$ did not give this appearance. In addition, amorphous aggregates were also apparent in the electron micrographs of the oxidized actin, as seen in our previous studies (*16*, *17*). Longer (15 min) copper-catalyzed air oxidation of the filaments on EM grids resulted in their destruction and complete conversion into aggregates (data not shown). In solution, at higher protein concentration and lower $CuSO_4$ to actin molar ratios, the cross-linking of F-actin was slower, reaching completion in 25−35 min. These observations suggest that filament destabilization and severing can occur through changes in the conformation of the hydrophobic loop 262−274, resulting from actin filament dynamics.

Disulfide Locking of the Hydrophobic Loop in F-actin Releases Rhodamine Phalloidin from Actin. We showed previously (*16*) that the fungal toxin phalloidin greatly increased the polymerization of $(LC)_2CA$ actin by stabilizing the lateral contacts and the structure of F-actin (*29*). We further suggested that the locking of the hydrophobic loop in the $(LC)_2CA$ F-actin in a monomer-like conformation with a disulfide bond might perturb the phalloidin binding site environment. If this premise is correct, the structural perturbations should lead to a release of phalloidin from the actin and a weakening of interprotomer contacts, leading to destabilization of the filament. To test this hypothesis, we assessed the ability of disulfide cross-linking between C180 and C269 $(LC)_2CA$ to release rhodamine phalloidin from filaments composed of this actin. To this end, 10 μM DTT-free $(LC)_2CA$ F-actin (in MOPS buffer containing 3.0 mM $MgCl_2$) was stabilized with a phalloidin/rhodamine phalloidin mixture and disulfide cross-linked at room temperature in a spectrofluorometer quartz cell, using 10 μM $CuSO_4$ to catalyze the air oxidation reaction. Aliquots of the reaction were analyzed on 7.5% SDS−PAGE gels while rhodamine phalloidin release was monitored via the decrease in rhodamine phalloidin fluorescence at 575 nm (Figure 2). Our results show that the disulfide locking of the hydrophobic loop in F-actin releases rhodamine phalloidin from actin. The rhodamine phalloidin release and C180−C269 cross-linking are virtually completed in 30−40 min. EM observations confirmed the destruction of filaments in the sample oxidized for 35 min (Figure 2B).

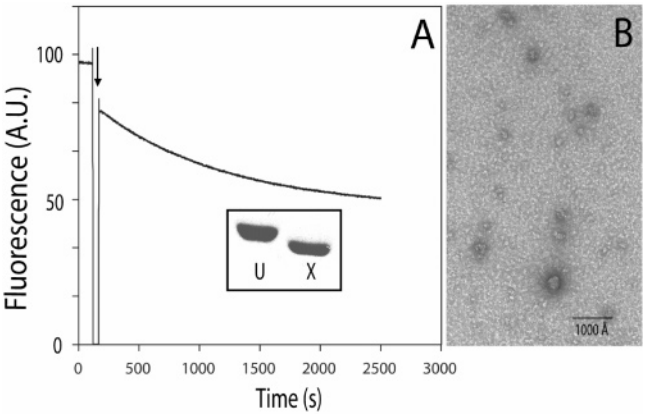

FIGURE 2: Disulfide cross-linking of C180−C269 in $(LC)_2CA$ F-actin and rhodamine phalloidin release. (A) Rhodamine phalloidin release from F-actin as monitored via a decrease in rhodamine fluorescence at 575 nm. At the time indicated by an arrow, 10 μM $CuSO_4$ was added to F-actin stabilized with a phalloidin/rhodamine phalloidin mixture to catalyze the disulfide cross-linking of C180 to C269. Inset: SDS−PAGE evidence for complete disulfide cross-linking of $(LC)_2CA$ actin after a 35 min copper-catalyzed oxidation reaction. Key: U, un-cross-linked actin; X, cross-linked actin. (B) Representative electron micrograph of the cross-linked F-actin. The bar corresponds to 1000 Å. Disulfide cross-linking (35 min) and rhodamine phalloidin release from F-actin resulted in filament destruction and conversion into aggregates.

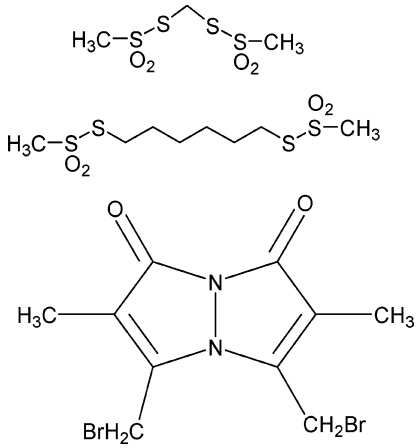

FIGURE 3: Structures of bis(methanethiosulfonate) (MTS-1, MTS-6) and dibromobimane (DBB) cross-linking reagents used in this work.

The Hydrophobic Loop 262−274 Fluctuates between the Detached and Parked Positions in both G- and F-actin. Earlier we showed that blocking the motion of the hydrophobic loop (262−274) in G-actin prevents normal filament formation and destabilizes existing filaments (*16*). These observations suggest a dynamic nature of the loop. One of the main goals of this study was to assess the range of proposed dynamic motions of the hydrophobic loop in G- and F-actin. To this end, we used increasing length (5.4−12.1 Å) flexible cross-linking reagents (MTS-1, -3, -4, -6, and -8) as molecular rulers. More rigid cross-linkings with DBB (4.4 Å) and direct disulfide bond formation between C180 and C269 (zero span cross-linking) were also used in these experiments. The structures of MTS-1, MTS-6, and DBB cross-linkers are shown in Figure 3. The MTS, DBB, and disulfide cross-linking experiments were carried out on the G and F forms of $(LC)_2CA$ actin in solution, as described

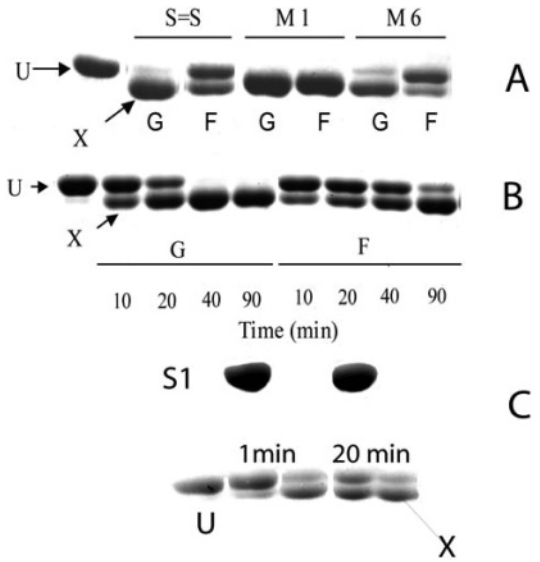

FIGURE 4: SDS−PAGE patterns of cross-linking of $(LC)_2CA$ F-actin. Actin oxidation and cross-linking were carried out as described in Experimental Procedures. (A) Disulfide (S═S) and MTS (M1 and M6) $(LC)_2CA$ actin cross-linked for 1 min. Key: G, G-actin; F, F-actin; U, un-cross-linked actin; X, cross-linked actin; M1, MTS-1 cross-linked actin; M6, MTS-6 cross-linked actin. Copper-catalyzed air oxidation of $(LC)_2CA$ G-actin for 1 min at room temperature resulted in its complete transformation into cross-linked species (with higher electrophoretic mobility on SDS−PAGE). Shorter incubation times produced two populations of $(LC)_2CA$ actin, with mobilities of the oxidized and unoxidized protein. In the case of F-actin, the oxidation reaction was significantly slower. The cross-linking reaction was faster with the short length MTS-1 (5.4 Å) than with the longer length MTS-4 (7.8 Å), MTS-6 (9.6 Å), and MTS-8 (12.1 Å) reagents (data not shown). (B) DBB cross-linking of $(LC)_2CA$ F-actin. (C) Disulfide cross-linking of F-actin in the presence of S1. F-actin (10 μM) was cross-linked at room temperature for 1 and 20 min in the absence and presence of S1 (10 μM DTT free). The oxidation was catalyzed by 5.0 μM $CuSO_4$.

in Experimental Procedures. Cross-linking experiments (Figure 4A) revealed that the hydrophobic loop is mobile and explores different conformations in G- and F-actin. The loop fluctuates from a parked state, captured by disulfide cross-linking, to detached conformations, captured by the longer span cross-linking reagents MTS-6 and MTS-8 (data not shown). Figure 4A shows that copper-catalyzed air oxidation of $(LC)_2CA$ G-actin resulted in its complete transformation after 1 min at room temperature into species with a higher electrophoretic mobility on SDS−PAGE (cross-linked actin). Shorter incubation times produced two populations of $(LC)_2CA$ actin with the mobilities of the oxidized and unoxidized protein. In the case of F-actin, the rate of the disulfide cross-linking was significantly slower; ~50% of F-actin was cross-linked after 4 min. The cross-linking reaction was faster (Figure 4*A*, lane M1) with the shorter length MTS-1 (5.4 Å) than with the longer length MTS-6 (9.6 Å) and MTS-8 (12.1 Å) (data not shown) reagents. The slow cross-linking of F-actin by MTS reagents and a disulfide bond suggests decreased loop flexibility in F-actin. As with the other reagents, the rate of cross-linking C180 to C269 by DBB (4.4 Å) was also slower in F-actin than in G-actin (Figure 4B). Only ~50% of the F-actin was cross-linked after 40 min. In contrast to F-actin, G-actin was completely cross-linked by DBB within 40 min. These results support our premise that the hydrophobic loop 262−274 is

mobile in F-actin, but less than in G-actin, fluctuating between the detached and parked conformations.

S1 and Tropomyosin Inhibit the Disulfide and DBB Cross-Linking of F-actin. It is well-known that skeletal muscle myosin subfragment 1 (S1) can induce the polymerization of G-actin into decorated filaments (*30*, *31*). We showed previously that S1 was unable to polymerize the cross-linked $(LC)_2CA$ G-actin into normal filaments (*16*). Here we explored how S1 and tropomyosin (Tm), which stabilize actin filaments, affect the disulfide and DBB cross-linking of the hydrophobic loop to the actin protomer surface in filaments. To this end, $(LC)_2CA$ F-actin (10 μM) was cross-linked at room temperature in the presence of 10 μM DTT-free S1 or 2.0 μM Tm, as described in Experimental Procedures. In both cases (disulfide and DBB) the rates of cross-linking were much higher in the absence of the actin binding proteins. In the presence of S1 (Figure 4C), after 1 min of copper-catalyzed air oxidation most of the F-actin ($\sim$95%) remained un-cross-linked. Longer oxidation time (20 min) in the presence of S1 yielded two populations of actin: $\sim$45% un-cross-linked and $\sim$55% cross-linked. We observed a similar inhibitory effect of Tm on the cross-linking reaction (data not shown). These results demonstrate that S1 and Tm inhibit the disulfide and DBB cross-linking of F-actin, suggesting that the stabilization of the F-actin structure by these proteins involves considerable inhibition of the hydrophobic loop fluctuations.

Cross-Linking of C180 to C269 in G- and F-actin with Reagents of Increasing Length Causes Decreasing Filament Impairment. We previously showed that linking C180 to C269 in G-actin blocked filament formation, resulting in its conversion into amorphous aggregates. This behavior demonstrates a need for a mandatory detachment of the hydrophobic loop during the G- to F-actin transition. We showed earlier in this work that the same reaction in F-actin resulted in the destabilization, severing, and breaking of the actin filament. These observations raised an interesting question: Does constraining the motion of the hydrophobic loop in G-actin by reagents with longer and more flexible cross-linking span block filament formation or cause destabilization and/or filament impairment? We were also interested in estimating the distances between these cysteines (C180−C269) that favor a stable filament structure. To answer these questions, we examined the effects of cross-linking C180 to C269 by a series of increasingly longer cross-linking reagents [zero span, DBB (4.4 Å), MTS-1 (5.4 Å), and MTS-6 (9.6 Å)] on actin filament stability. Actin samples were cross-linked in solution as described in Experimental Procedures and then spread on EM grids to check for impairment of the filament structure. Filament formation of DBB, MTS-1, and MTS-6 cross-linked actin was monitored also via light scattering measurements as described in Experimental Procedures.

Electron microscopy (Figure 5A) revealed that MTS-6 (9.6 Å) cross-linking had no significant effect on filament structure when compared to filaments formed by un-cross-linked actin. Light scattering measurements showed no difference in the rate of filament formation between un-cross-linked and MTS-1 and MTS-6 cross-linked G-actin (data not shown). Electron microscopy showed that, in the case of MTS-1, the cross-linked actin filaments were normal in appearance (Figure 5B) but were shorter than the control

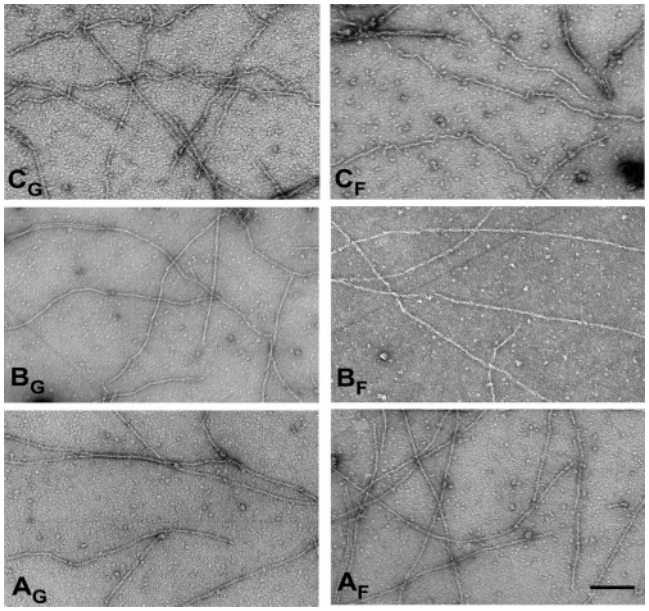

FIGURE 5: Electron micrographs of DBB and MTS cross-linked $(LC)_2CA$ actin: A_G, F-actin formed from G-actin cross-linked with MTS-6; A_F, F-actin cross-linked with MTS-6; B_G, F-actin formed from MTS-1 cross-linked G-actin; B_F, F-actin cross-linked with MTS-1; C_G, F-actin formed from G-actin cross-linked with DBB; C_F, F-actin cross-linked with DBB. The bar represents 1000 Å. Actin cross-linkings were carried out as described in Experimental Procedures.

filaments (data not shown). The light scattering profile of polymerization of DBB-cross-linked G-actin was different from that of un-cross-linked actin, suggesting some destabilization/impairment of the filament structure, as well as formation of nonspecific aggregates (data not shown). EM confirmed this suggestion: cross-linking C180 to C269 by DBB (4.4 Å) in either G- or F-actin (Figure 5C) resulted in shorter and less stable filaments. These cross-linked filaments appeared less smooth than the control filaments and were wavy and partially broken as well as occasionally converted into aggregates.

A molecular dynamic simulation modeling (see Experimental Procedures) of the 262−274 loop after C180−C269 cross-linking revealed that whereas disulfide locking of the loop resulted in its twisted conformation, MTS-6 (9.6 Å) and DBB (4.4 Å) cross-linkings had no significant effect on the conformation of the loop when compared with un-cross-linked actin (data not shown).

The fact that only cross-linking with the MTS-6 (9.6 Å) reagent did not impair actin polymerization and filament structure suggests that the distance between cysteines 180−269 which favors a stable filament structure may be within the range of 9−10 Å.

Electron Paramagnetic Resonance Measurements with Nitroxide Spin-Labeled $(LC)_2CA$ Actin Reveal Strong Spin−Spin Coupling and a Similar Mean Interspin Distance ($\sim$10 Å) in G- and F-actin. We used spin-labeled G- and F-actin to determine the interspin distance distribution between two cysteine residues (180−269) in $(LC)_2CA$ actin and to probe the dynamics of the hydrophobic loop. Labeling stoichiometry of these samples was checked by MALDI mass spectrometry, revealing a 2:1 mole ratio of the spin probe to actin. In both G-actin and F-actin (Figure 6) the nitroxide groups are clearly close enough to each other to affect the

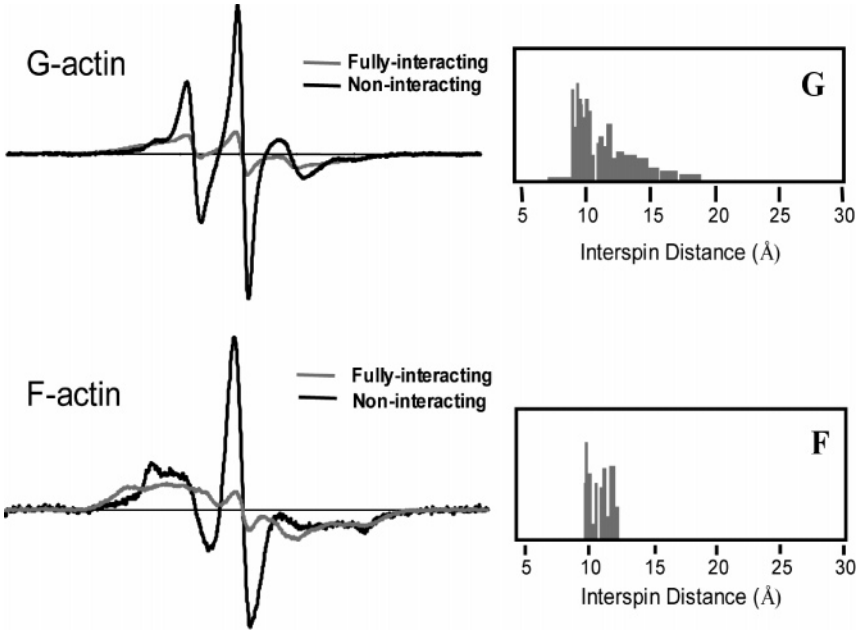

FIGURE 6: EPR spectra of $(LC)_2CA$ actin: G-actin (top panel) and F-actin (bottom panel). In the EPR spectra (left side), the spectrum of the MTSL-labeled actin mutant (double, in gray) is compared to the spectrum of actin reacted with a 1:2 molar ratio mixture of paramagnetic MTSL and diamagnetic spin-labels (sum of singles, in black). The spectra are displayed after correction for baseline artifacts and the unbound spin-labels. Interspin distance panels (right side) show the distribution of interspin distances between spin probes at C180 and C269 in G- (top) and F-actin (bottom).

EPR spectrum, as evidenced by strong spectral broadening and a corresponding reduction in intensity. The right side panels in Figure 6 show the distance distributions obtained from a best fit to the fully interacting spectrum obtained as the convolution of a sum of Pake functions with the noninteracting spectrum. The distribution of distances in G-actin is quite broad, and slightly bimodal, spreading from 9 to 18 Å. This spread narrows considerably in F-actin (Figure 6). These observations are consistent with molecular dynamic simulation modeling of the spin-labeled actin (see Experimental Procedures). The possible distances between the two spin probes in the modeling were found to be in the range of 6.2−25.2 Å. Whereas the pairs of labels in G-actin adopt at least two or three different relative conformations (Figure 6), all of the label pairs in F-actin are in a tight distribution at a relatively close distance (9−12 Å).

EPR spectra of the fully spin-labeled L180C/L269C/C374A actin showed a marked restriction of the motion in the environment around the spin-labeled sites upon polymerization. To resolve the specific contributions to this result, we examined the EPR spectra of singly labeled actin mutants (Figure 7).

EPR of a single cysteine mutant L269C/C374A actin revealed a significant difference in mobility of the spin probe between G- and F-actin (Figure 7), suggesting that most of the difference in mobility of the hydrophobic loop seen in $(LC)_2CA$ actin was from labels at the C269 site. The spin probe at C269 in the single cysteine F-actin was extremely immobile (Figure 7). The direction and magnitude of the change correlate well with the change seen in the double cysteine mutant: polymerization restricts the motion of the C269 spin-label.

In L180C/C374A actin with one labeled cysteine at position 180, EPR measurements show only a small difference between G- and F-actin spectra. Although the trend of the line shape changes is similar to those seen in the doubly labeled actin mutant, the magnitude of the difference is much smaller. This is in contrast to the large differences upon polymerization shown above for EPR spectra of actin with a single labeled cysteine at position 269.

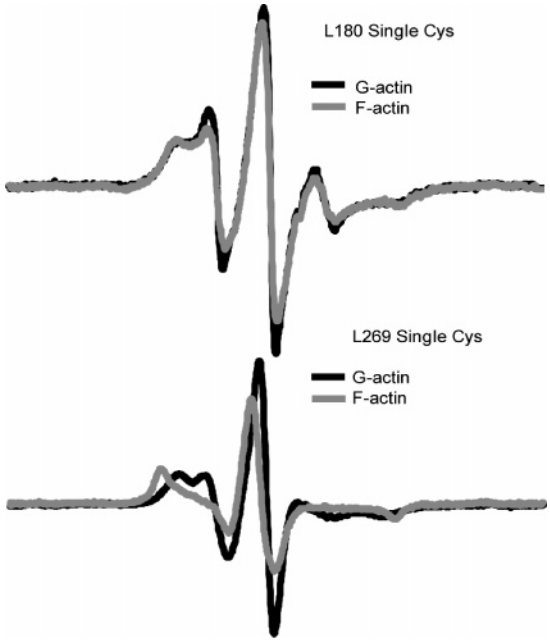

FIGURE 7: EPR spectra of single spin-labeled actin. In each of the panels, G-actin (black) and F-actin (gray) EPR spectra are compared. The spectra are displayed after correction for baseline artifacts and unbound spin-labels. EPR spectra for L180C (top panel) show only small differences between monomer and filamentous actin. In contrast, the spectra of L269C (bottom panel) show that spin-labels at this position are extremely sensitive to structural changes upon filament formation, displaying greatly hindered motion in F-actin in comparison to G-actin.

To confirm the conclusion that spin-labels at position 180 are only weakly sensitive to structural changes induced by

polymerization, while those at position 269 are very strongly sensitive to filament formation, we modeled the EPR spectrum of the doubly labeled mutant. Using linear combinations of the two single cysteine actin spectra, we satisfactorily fit the diluted doubly labeled spectrum (see Experimental Procedures) with the residual spin−spin interactions removed by spectral subtraction. This supports the conclusion that most of the polymerization-induced rigidity seen by EPR is detected by spin-labels at C269.

DISCUSSION

The focus of this study was to assess the extent of the dynamic motions of the hydrophobic loop between subdomains 3 and 4 of actin. In Holmes' original model of the actin filament, this loop was predicted to detach from the surface of the protein and to extend across the interstrand cleft to form a cross-strand bridge. Such a change would impart structural stability to the filament. However, hydrophobic loop motion and its insertion into the opposite strand are not required in the recent F-actin model based on crystal contacts in the actin dimer (*32*).

If loop extension, accompanied by its docking in a hydrophobic pocket, were critical for filament stability, one might not expect the loop to exhibit dynamic properties within the actin filament. Yet, following F-actin formation, zero-length cross-linking of C180 to C269 occurred and resulted in filament disruption (*16, 17*). What these results did not reveal was the extent of loop movement that was required for filament formation, the extent of loop mobility in F-actin, and the extent to which actin binding proteins could affect loop movement in the filament interior. Such questions are addressed in this study.

Our results with the cross-linkers of increasing length reaffirmed that the loop in F-actin can exist in both detached and parked states. More importantly, they provided insight into the degree of freedom the loop must have for stable filament formation. A distance of 9.6 Å between the sulfurs on C180 and C269 provided sufficient flexibility for that purpose. Further curtailment of this inter-sulfur length produces increasing strain in the filament that first results in shortened filament length and then distortions in filament morphology. Thus, the conformational flexibility of actin allows the filament to withstand strain and local distortions and still remain at least partly intact. Such flexibility is likely to be important for the cytoskeleton to be able to work with the array of actin binding proteins it experiences without disintegrating from the changes imposed upon it. In the experiments with the series of MTS reagents, the decreased rate of cross-linking with increasing length is best explained by decreased collisional frequency of the active residues of the reagents with the target sulfurs due to a greater volume being sampled by the ends of the cross-linker.

Disulfide cross-linking of the two sulfurs led to filament disruption, further demonstrating that local, intrinsically unstable conformations of actin filaments, which are products of loop flexibility, exist in the filament ensemble perhaps infrequently and are captured by the cross-linking reaction. A series of EM studies of Egelman and co-workers presented evidence for alternative, tilted forms of the filament (*17, 33, 34*). Filament-destabilizing reagents or proteins (such as tetramethylrhodamine or cofilin) increase the population of tilted F-actin, and it has been suggested that this form might be an intermediate not only in filament disruption but also in filament formation and maturation. If so, intermediate forms such as these may account, in part, for the preference of proteins such as the Arp2/3 complex for newly polymerized actin.

The inhibition of cross-linking between C180 and C269 by two filament stabilizing proteins, S1 and tropomyosin, underscores the ability of proteins binding on the filament exterior to exert allosteric changes that affect domain movement in the filament interior. On the basis of our work, each of these proteins stabilizes F-actin, at least in part, by decreasing the extent to which the G-parked loop conformations can be populated within the filament. In the context of muscle contraction, such filament stabilization and restriction of loop movement would lead to a greater efficiency in the transduction of contractile force generated by the myosin ATPase activity.

A particularly interesting result in these tropomyosin/myosin experiments is the similar extent to which these two proteins exert their effect on the 262−274 loop. This similarity differs from the results of two previous observations. Feng et al. (*10*) demonstrated that myosin S1, but not tropomyosin, affected the fluorescent behavior of a pyrene attached to residue 265 in the loop, and it has long been known that myosin, but not tropomyosin, can affect the fluorescence of pyrene attached to C374. However, in these last two examples, the fluorescence changes observed depend not only on the movement of the loop caused by the actin binding proteins but on the changes induced in structures that interact with the loop probes as well. Loop movement, per se, in each of these instances might have been similar.

Our use of EPR to assess loop behavior represents a novel application of site-directed EPR to the study of actin filament dynamics. The population of loop states with interspin distances of 9−18 Å in G-actin is reduced to a much more tightly defined population with interspin distances of 9−12 Å in F-actin. Such a reduction is consistent with a filament-induced restriction in loop flexibility indicated by the observed differences in the rates of cross-linking between G- vs F-actin. Furthermore, the agreement between the optimal cross-linking distance and the mean interspin distance (∼10 Å) in F-actin lends credence to this value. Experiments with actins containing single cysteines at either position 180 or position 269 confirm it is the loop residue, and not C180, that is primarily responsible for the inter-sulfur distance changes.

The 9−10 Å interspin distance is close to the distance predicted for the Holmes (*7*) and the new (*32*) models of F-actin structure. More importantly, the same mean interspin distance is found in G-actin, suggesting no major rearrangement of loop 262−274 upon actin polymerization, except for its reduced mobility and more confined conformational space (i.e., narrower distance distribution). Recent EM work (*35*) suggests an increased density where the extended loop is expected to be. However, insertion of bulky hydrophobic probes to the loop does not affect actin polymerization, in contradiction to the need for complete and stable loop extension (*10, 15*). Convincing demonstration of the docking of the loop in a hydrophobic pocket in the opposing strand of the filament would require evidence of a direct interaction such as that provided by cross-linking. Despite repeated

attempts by us and others to generate such data (unpublished results), such evidence has not been obtained.

Our results point to a situation in which multiple conformations of a single filament, let alone a collection of filaments, exist at any time. Consistent with the EPR measurements of interspin distances in F-actin, some of the transient and less frequent conformations, when trapped by cross-linking, destabilize the filaments. We propose that severing proteins may take advantage of such states. Clearly, a mechanistic understanding of the allosteric regulation of the actin filament by different actin binding proteins is required to clarify the manner in which these proteins interact with actin to produce the desired biological effect. Such an understanding requires an assessment of the conformational flexibility in the filament associated with mobile elements within the actin monomer. Continued studies along the lines of those performed here will produce the knowledge needed for the delineation of these regulatory pathways.

ACKNOWLEDGMENT

We thank Drs. Joe Loo and Rachel Ogorzalek Loo for expert assistance with MALDI mass spectrometry and Mai Phan for technical assistance with EM.

REFERENCES

1. Small, J. V., Anderson, K., and Rottner, K. (1996) Actin and the coordination of protrusion, attachment and retraction in cell crawling, *Biosci. Rep. 16*, 351−368.
2. Kreis, T., and Vale, R. (Editors) (1999) *Guidebook to the Cytoskeletal and Motor Proteins*, 2nd ed., Oxford University Press, Oxford, U.K.
3. Pollard, T. D., Blanchoin, L., and Mullins, R. D. (2000) Molecular mechanisms controlling actin filament dynamics in nonmuscle cells, *Annu. Rev. Biophys. Biomol. Struct. 29*, 545−576.
4. Dos Remedios, C., Chabra, D., Kekic, M., Dedova, I., Tsubakihara, M., Berry, D., and Nosworthy, N. (2003) Actin binding proteins: regulation of cytoskeletal microfilaments, *Physiol Rev. 83*, 433−473.
5. Holmes, K. C., Popp, D., Gebhard, W., and Kabsch, W. (1990) Atomic model of the actin filament, *Nature 347*, 44−49.
6. Lorenz, M., Popp, D., and Holmes, K. C. (1993) Refinement of the F-actin model against X-ray fiber diffraction data by the use of a directed mutation algorithm, *J. Mol. Biol. 234*, 826−836.
7. Holmes, K. C., Angert, I., Kull, F. J., Jahn, W., and Schroder, R. R. (2003) Electron cryo-microscopy shows how strong binding of myosin to actin releases nucleotide, *Nature 425*, 423−427.
8. Kabsch, W., Mannherz, H. G., Suck, D., Pai, E. F., and Holmes, K. C. (1990) Atomic structure of the actin:DNase I complex, *Nature 347*, 37−44.
9. Tirion, M. M., ben-Avraham, D., Lorenz, M., and Holmes, K. C. (1995) Normal modes as refinement parameters for the F-actin model, *Biophys. J. 68*, 5−12.
10. Feng, L., Kim, E., Lee, W. J., Miller, C., Kuang, B., Reisler, E., and Rubenstein, P. A. (1997) Fluorescence probing of yeast actin subdomain 3/4 hydrophobic loop 262−274, *J. Biol. Chem. 272*, 16829−16837.
11. Kuang, B., and Rubenstein, P. A. (1997) Beryllium fluoride and phalloidin restore polymerizability of a mutant yeast actin (V266G, L267G) with severely decreased hydrophobicity in a subdomain 3/4 loop, *J. Biol. Chem. 272*, 1237−1247.
12. Wen, K., Kuang, B., and Rubenstein, P. A. (2000) Tropomyosin-dependent filament formation by a polymerization-defective mutant yeast actin (V266G, L267G), *J. Biol. Chem. 275*, 40594−40600.
13. Kim, E., Wriggers, W., Phillips, M., Kokabi, K., Rubenstein, P. A., and Reisler, E. (2000) Cross-linking constraints on F-actin structure, *J. Mol. Biol. 299*, 421−429.
14. Kim, E., and Reisler, E. (2000) Intermolecular dynamics and function in actin filaments, *Biophys. Chem. 86*, 191−201.
15. Musib R., Wang, G., Geng, L., and Rubenstein, P. A. (2002) Effect of polymerization on the subdomain 3/4 loop of yeast actin, *J. Biol. Chem. 277*, 22699−22709.
16. Shvetsov, A., Musib, R., Phillips, M., Rubenstein, P., and Reisler, E. (2002) Locking the hydrophobic loop 262−274 to G-actin surface by a disulfide bridge prevents filament formation, *Biochemistry 41*, 10787−10793.
17. Orlova, A., Shvetsov, A., Galkin, V. E., Kudryashov, D. S., Rubenstein, P. A., Egelman, E. H., and Reisler, E. (2004) Actin-destabilizing factors disrupt filaments by means of a time reversal of polymerization, *Proc. Natl. Acad. Sci. U.S.A. 101*, 17664−17668.
18. Berliner, L. J., Grunwald, J., Hankovszky, H. O., and Hideg, K. (1982) A novel reversible thiol-specific spin label: papain active site labeling and inhibition, *Anal. Biochem. 119*, 450−455.
19. Hideg, K., Hankovszky, H. O., Lexs, L., and Kulcsar, G. Y. (1980) Nitroxyls; VI. Synthesis and reactions of 3-hydroxymethyl-2,2,5,5-tetramethyl-2,5-dihydropyrrole-1-oxyl and 3-formyl derivatives, *Synthesis*, 911−914.
20. Chen, X., Cook, R. K., and Rubenstein P. A. (1993) Yeast actin with a mutation in the "hydrophobic plug" between subdomains 3 and 4 (L266D) displays a cold-sensitive polymerization defect, *J. Cell Biol. 123*, 1185−1195.
21. Weeds, A. G., and Pope, B. (1977) Studies on the chymotryptic digestion of myosin. Effects of divalent cations on proteolytic susceptibility, *J. Mol. Biol. 111*, 129−157.
22. Smillie, L. B. (1982) Preparation and identification of alpha- and beta-tropomyosins, *Methods Enzymol. 85* (Part B), 234−241.
23. Laemmli, U. K. (1970) Cleavage of structural proteins during the assembly of the head of bacteriophage T4, *Nature 227*, 680−685.
24. Kim, E., Phillips, M., Hegyi, G., Muhlrad, A., and Reisler, E. (1998) Intrastrand cross-linked actin between Gln-41 and Cys-374. II. Properties of cross-linked oligomers, *Biochemistry 37*, 17793−17800.
25. Hubbell, W. L., Froncisz, W., and Hyde, J. H. (1987) Continuous and stopped flow EPR spectrometer based on a loop gap resonator, *Rev. Sci. Instrum. 58*, 1879−1886.
26. Altenbach, C., Oh, K. J., Trabanino, R. J., Hideg, K., and Hubbell, W. L. (2001) Estimation of inter-residue distances in spin labeled proteins at physiological temperatures: experimental strategies and practical limitations, *Biochemistry 40*, 15471−15482.
27. Rabenstein, M. D., and Shin, Y. K. (1995) Determination of the distance between two spin labels attached to a macromolecule, *Proc. Natl. Acad. Sci. U.S.A. 92*, 8239−8243.
28. Pake, G. E. (1948) Nuclear resonance absorption in hydrated crystals: Fine structure of the proton line, *J. Chem. Phys. 16*, 327−336.
29. Steinmetz, M., Stoffler, D., Muller, S., Jahn, W., Wolpensinger, B., Goldie, N., et al. (1998) Evaluating atomic models of F-actin with an undecagold-tagged phalloidin derivative, *J. Mol. Biol. 276*, 1−6.
30. Miller, L., Phillips, M., and Reisler, E. (1988) Polymerization of G-actin by myosin subfragment 1, *J. Biol. Chem. 263*, 1996−2002.
31. Carlier, M.-F., Didry, D., Erk, I., Lepault, J., and Pantaloni, D. (1994) Myosin subfragment-1-induced polymerization of G-actin. Formation of partially decorated filaments at high actin-S1 ratios, *J. Biol. Chem. 269*, 3829−3837.
32. Kudryashov, D. S., Sawaya, M. R., Adisetiyo, H., Norcross, T., Hegyi, G., Reisler, E., and Yeates, T. O. (2005) The crystal structure of a cross-linked actin dimer suggests a detailed molecular interface in F-actin, *Proc. Natl. Acad. Sci. U.S.A. 102*, 13105−13110.
33. Galkin, V. E., Orlova, A., Lukoyanova, N., Wriggers, W., and Egelman, E. H. (2001) Actin depolymerizing factor stabilizes an existing state of F-actin and can change the tilt of F-actin subunits, *J. Cell Biol. 153*, 75−86.
34. Egelman, E. H. (2004) Acrosomal actin: twists and turns of a versatile filament, *Curr. Biol. 14*, R559−R961.
35. Schmid, M. F., Sherman, M. B., Matsudaira, P., and Chiu, W. (2004) Structure of the acrosomal bundle, *Nature 431*, 104−107.

BI052558V